Single-photon superradiant emission rate scaling for atoms trapped in a photonic waveguide

Yao Zhou, Zihao Chen, and Jung-Tsung Shen
Department of Electrical and System Engineering, Washington University in St. Louis, St. Louis, Missouri 63130, USA
(Received 23 December 2016; published 21 April 2017)

A recent experiment reveals the linear scaling property of the superradiant emission rate for a trapped atom cloud that is excited by weak and short light pulses. We adopt a real-space approach to numerically demonstrate that such a linear scaling law can be interpreted as single-photon superradiance, in both the time domain and the frequency domain. The dependence of the single-photon superradiant emission rate on the distance between atoms is investigated. We further study the single-photon superradiance for artificial atoms that have deviations in transition frequencies and decay rates.

DOI: 10.1103/PhysRevA.95.043832

The collective spontaneous emission of a cloud of dilute excited atoms, wherein atoms are considered as interacting independently with the radiation field, obeys an exponential law characterized by a time scale, τ_{sp}, equal to the reciprocal of the single-atom decay rate, Γ_1 [1]. When the density of atoms is large enough, the excited atom cloud is radiatively damped in a short radiation burst, with a time scale of the order of τ_{sp}/N (N is the number of atoms). The peak intensity of the radiation is proportional to N^2. This phenomenon is called superradiance and was first theoretically analyzed by Dicke [2]. In addition to the multiphoton superradiance, a single-photon radiation speed-up that is much faster than the single-atom spontaneous emission can also occur when a single photon is stored uniformly in an N-atom cloud. Such a single-photon superradiance has recently attracted considerable attention [3–7], as the effective strong atom-photon coupling is promising for ultrafast quantum optical devices for high-speed quantum networks [8–12]. For the time-reversed process of capturing an incident single photon by the atom cloud, the capturing time could be substantially reduced and the excited state of the atom ensemble can be designed to be maximally entangled. These features are important for efficient quantum information storage and for quantum communication [13].

The dependence of the effective decay rate Γ_N on the atom number N, which is called the superradiant emission rate scaling, is an important measure of superradiance. Superradiance from atomic gas was experimentally observed decades ago [14,15]. However, due to the challenge of precisely controlling the atom number, these experiments could not directly check the scaling law. Recently, by trapping atoms in a single-mode photonic crystal waveguide (SMPCW), the superradiant emission rate scaling has been experimentally verified [16,17]. In these experiments, the average number is controlled ($\overline{N} < 3$ in these experiments), and weak and short excitation pulses (with an average photon number much less than one per pulse) are injected in the PCW to excite the atoms. By measuring the output intensity and transmission spectrum for a varying average atom number (controlled by changing the hold time after loading), the dependence of the total decay rate on the atom number can be determined. In this article, we numerically demonstrate both in the time domain and the frequency domain that the scaling law in this scenario can be interpreted as single-photon superradiance. We also investigate the single-photon scaling law for an ensemble of quantum emitters when their locations are spatially distributed or when the transition frequencies or the coupling strengths vary.

Figure 1 depicts the system: an ensemble of N atoms trapped in a SMPCW [17]. Each atom is a two-level system, initially at its ground state. The waveguide is single mode so that multimode interferences, which in general degrade the quantum coherence, are absent. The electric field is sharply peaked at the center of the unit cells. Only atoms trapped at the center of the unit cell couple to the optical field, and the coupling strengths are approximately considered identical. The off-centered atoms are neglected. To simulate the process, we send in a single-photon Gaussian wave packet with a spatial width, σ_p, from the far left. By numerically evolving the system dynamics in time, the optical responses are determined. Specifically, the system is modeled by the following Hamiltonian [18]:

$$\begin{aligned} H = & \int dx \left[-i v_g \hbar c_R^\dagger(x) \frac{\partial}{\partial x} c_R(x) + i v_g \hbar c_L^\dagger(x) \frac{\partial}{\partial x} c_L(x) \right] \\ & + \sum_{n=1}^{N} [\hbar(\Omega_{ne} - i\gamma_n) a_{ne}^\dagger a_{ne} + \hbar \Omega_{ng} a_{ng}^\dagger a_{ng}] \\ & + \int dx \hbar V \sum_{n=1}^{N} \delta(x - x_n) [c_R^\dagger(x) a_{ng}^\dagger a_{ne} + c_R(x) a_{ne}^\dagger a_{ng} \\ & + c_L^\dagger(x) a_{ng}^\dagger a_{ne} + c_L(x) a_{ne}^\dagger a_{ng}]. \end{aligned} \tag{1}$$

The first two terms describe the freely propagating photons in the waveguide with a group velocity, v_g. $c_R(x)$ [$c_R^\dagger(x)$] is the annihilation (creation) operator for a right-moving photon at position x. $c_L(x)$ [$c_L^\dagger(x)$] is similarly defined for the left-moving photon. The third term describes the atoms. a_{ne} ($a_{ne}^\dagger$) and a_{ng} ($a_{ng}^\dagger$) are the annihilation (creation) operators of the excited and the ground state of the nth atom, respectively. Ω_{ne} and Ω_{ng} are the excited and the ground state frequency of the nth atom, respectively; $\Omega_n \equiv \Omega_{ne} - \Omega_{ng}$ is the transition frequency. The decay rate γ_n describes the decay into free space [19]. The remaining terms describe the photon-atom interaction, where V is the coupling strength. The single-atom decay rate $\Gamma_1 \equiv V^2/v_g$ describes the atomic decay into the waveguide [18]. It can be shown that the total atom decay rate of the nth atom is $\Gamma_1 + \gamma_n$ [20]. The general state of the entire

system is

$$|\Psi(t)\rangle = \int dx[\phi_R(x,t)c_R^\dagger(x) + \phi_L(x,t)c_L^\dagger(x)]|0,-\rangle + \sum_{n=1}^{N} e_n(t)e^{-i(\Omega_n - i\gamma_n)t}a_{ne}^\dagger a_{ng}|0,-\rangle, \quad (2)$$

where the vacuum state $|0,-\rangle \equiv |0\rangle \otimes |-_1\rangle \otimes \cdots \otimes |-_N\rangle$ has no photon in the waveguide and all atoms are at the ground state. $\phi_R(x,t)$ and $\phi_L(x,t)$ are the single-photon wave functions and $e_n(t)$ is the excitation amplitude of the nth atom.

It is often advantageous to map the atomic cloud with a single excitation onto an effective two-level system. Here we present such a mapping and discuss the criteria for the mapping to be valid. The state describing an effective two-level system interacting with a single photon is

$$|\overline{\Psi}(t)\rangle = \int dx[\overline{\phi}_R(x,t)c_R^\dagger(x) + \overline{\phi}_L(x,t)c_L^\dagger(x)]|0,\overline{-}\rangle + \overline{e}(t)e^{-i(\overline{\Omega}-i\overline{\gamma})t}\overline{a}_e^\dagger\overline{a}_g|0,\overline{-}\rangle, \quad (3)$$

where $|0,\overline{-}\rangle \equiv |0\rangle \otimes |\overline{-}\rangle$ is the vacuum state of the effective system, containing zero photons and the effective atom at ground state. The effective Hamiltonian is (excluding the photon part for brevity)

$$\overline{H} = \hbar(\overline{\Omega}_e - i\overline{\gamma})\overline{a}_e^\dagger\overline{a}_e + \hbar\overline{\Omega}_g\overline{a}_g^\dagger\overline{a}_g + \int dx\hbar\overline{V}\delta(x-\overline{x})[c_R(x)\overline{a}_e^\dagger\overline{a}_g + c_R^\dagger(x)\overline{a}_g^\dagger\overline{a}_e + c_L(x)\overline{a}_e^\dagger\overline{a}_g + c_L^\dagger(x)\overline{a}_g^\dagger\overline{a}_e], \quad (4)$$

where an overline is used to denote the corresponding terms in the effective system. It is mathematically convenient to describe the two systems in the same Hilbert space; thus we define $|\overline{-}\rangle \equiv |-\rangle$. We require that the two states [Eq. (2) and Eq. (3)] are asymptotically equal before and after scattering for any single excitation. That is, $|\Psi(t)\rangle \approx |\overline{\Psi}(t)\rangle$ for $t \to -\infty$ and $t \to \infty$ for the same single-photon input or for physically accessible spontaneous emission. The asymptotic condition ensures the same scattering matrix for both systems. The physically accessible spontaneous emission uniquely maps the excited state of the effective atom to a single state in the atom cloud (among many states of single excitation). By satisfying the asymptotic condition, we find a set of conditions and unique mappings between the parameters and the operators of the two systems. The conditions are the following: first, the size of the incident photon must be much larger than the atom cloud, i.e., the mapping is valid for single frequency, which is met in many experiments; second, $x_1 \leqslant \overline{x} \leqslant x_N$ and $x_n - \overline{x} \ll \sigma_p, \forall n$. The mappings are [21]

$$\overline{a}_e^\dagger\overline{a}_g = \sum_{n=1}^{N} e^{ik_0(x_n-\overline{x})}a_{ne}^\dagger a_{ng}/\sqrt{N}, \quad (5a)$$

$$\overline{V} = \sqrt{N}V, \quad (5b)$$

$$\overline{e}(t) = \sqrt{N}e^{-ik_0(x_n-\overline{x})}e_{na}(t), \quad \forall n, \quad (5c)$$

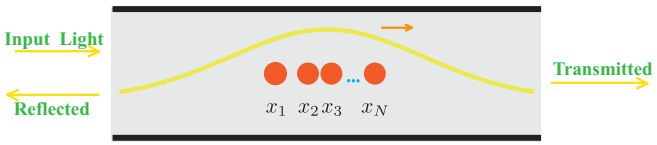

FIG. 1. Schematic of the system of trapped atoms (denoted by orange circles) in a single-mode waveguide. The single photon is injected from the left and interacts with the cloud of atoms. x_n is the position of the nth atom.

$$\overline{\Omega}_g = \sum_{n=1}^{N} \Omega_{ng}, \quad (5d)$$

$$\overline{\Omega} = \Omega_n, \quad \overline{\gamma} = \gamma_n, \quad \forall n, \quad (5e)$$

$$e^{2ik_0(x_n-\overline{x})} = 1, \quad \forall n, \quad (5f)$$

where approximation $e^{ik(x_n-\overline{x})} \approx e^{ik_0(x_n-\overline{x})}$ ($k_0 = \omega_0/v_g = 2\pi/\lambda$ is the center frequency of the photon) has been used. Equation (5b) immediately implies that the effective decay rate in the waveguide for the N-atom cloud Γ_N is enhanced by N-fold: $\Gamma_N = \overline{V}^2/v_g = N\Gamma_1$. Equations (5d) and (5e) indicate all atoms (including the effective atom) have the same transition frequency and dissipation rate. To satisfy Eq. (5f), we must have $x_n = x_1 + M_n\lambda/2$, and $\overline{x} = x_1 + \overline{M}\lambda/2$, where M_n and $\overline{M}$ are arbitrary integers (but still meet $x_n - \overline{x} \ll \sigma_p$); thus $e^{-ik_0(x_n-x_1)} = (-1)^{(M_n-\overline{M})}$.

One important consequence is that when single-photon superradiance occurs, the effective two-level system predicts a Lorentzian transmission spectrum with a full width at half maximum (FWHM) of $2(\gamma + N\Gamma_1)$, in contrast to $2(\gamma + \Gamma_1)$ of the single atom [20,22]. The broadening of the transmission spectrum has been suggested to be used for an atomic mirror [23]. We note that when the mappings are not valid, i.e., the set of Eqs. (5) is not satisfied, the transmission spectrum can be non-Lorentzian. In the following, to illustrate the effect of single-photon superradiance, we assume the atoms are lossless, i.e., $\gamma_n = 0, \forall n$.

When M_n are all even numbers, the single-photon superradiance can be compactly described [1]: The transition of a two-level system is mathematically equivalent to the flip of a spin-$\frac{1}{2}$ system, leading to the following relations: $a_{ng}^\dagger a_{ne} = \sigma_n^-$ and $a_{ne}^\dagger a_{ng} = \sigma_n^+$, where σ_n^- and σ_n^+ are the ladder operators of the nth atom. To describe the interaction between the photon and the atom cloud, when the atoms are in proximity to each other, or when M_n are even, collective ladder operators $\sigma^- = \sum_{n=1}^{N}\sigma_n^-$ and $\sigma^+ = \sum_{n=1}^{N}\sigma_n^+$ are defined. The state of the atom cloud thus is equivalent to the state of N spin-$\frac{1}{2}$ systems. The ground state of the cloud now is expressed as $|\frac{N}{2},-\frac{N}{2}\rangle$, and the absorption of a single photon raises it to $|\frac{N}{2},-\frac{N}{2}+1\rangle$, which is a symmetric multiatom state for the single-photon excitation. Here the atomic state is expressed in the angular momentum representation $|J,Z\rangle$, where J is the total angular momentum and Z is the z component. The general state of the atom cloud is $|\text{Cloud}(t)\rangle = C_1(t)|\frac{N}{2},-\frac{N}{2}+1\rangle + C_0(t)|\frac{N}{2},-\frac{N}{2}\rangle$, where now $C_1(t)$ is the effective atom excitation $\overline{e}(t)$ in Eq. (3) (differs by a trivial phase

$e^{-i\bar{\Omega}t}$). Equating the photon emission rate to the decreasing rate of the excited state population of the atoms, $d|C_1(t)|^2/dt = -\Gamma_1\langle \text{Cloud}(t)|\sigma^+\sigma^-|\text{Cloud}(t)\rangle$, we obtain $|C_1(t)|^2 = e^{-N\Gamma_1 t}$ by the equation, with the initial conditions $C_1(t=0)=1$ and $C_0(t=0)=0$. That is, the cloud is initially in the single-photon excitation state $|\frac{N}{2},-\frac{N}{2}+1\rangle$. We note that the exact scaling $\Gamma_N = N\Gamma_1$ is a direct consequence from the symmetric excited state of the atom cloud and also from the phase coherence in the interaction (M_n are even). Considering that each atom cannot be distinguished in this scenario, superradiance can also be interpreted as the interference of photon paths [24].

With the physical insights, we now present the numerical results. By applying the Schrödinger equation, we obtain the following equations of motion:

$$\frac{\partial}{\partial t}\phi_R(x,t) = -v_g\frac{\partial}{\partial x}\phi_R(x,t) - iV\Sigma_{n=1}^{N}\delta(x-x_n)e_{na}(t)e^{-i\Omega_n t},$$
$$\frac{\partial}{\partial t}\phi_L(x,t) = v_g\frac{\partial}{\partial x}\phi_L(x,t) - iV\Sigma_{n=1}^{N}\delta(x-x_n)e_{na}(t)e^{-i\Omega_n t},$$
$$\frac{\partial}{\partial t}e_{na}(t) = -iV[\phi_L(x_n,t)+\phi_R(x_n,t)]e^{i\Omega_n t}. \quad (6)$$

At $t=0$, a right-moving photon is launched from the left of the atom cloud. The single-photon wave form is $\phi_R(x,t=0) = (1/2\pi\sigma_p^2)^{1/4}e^{-\frac{(x-x_0)^2}{4\sigma_p^2}}e^{ik_0x}$, where $\sigma_p = 0.1v_g/\Gamma_1$, x_0 is the center of the photon wave form at $t=0$, which is chosen to be at the far left of the atom cloud (the specific value

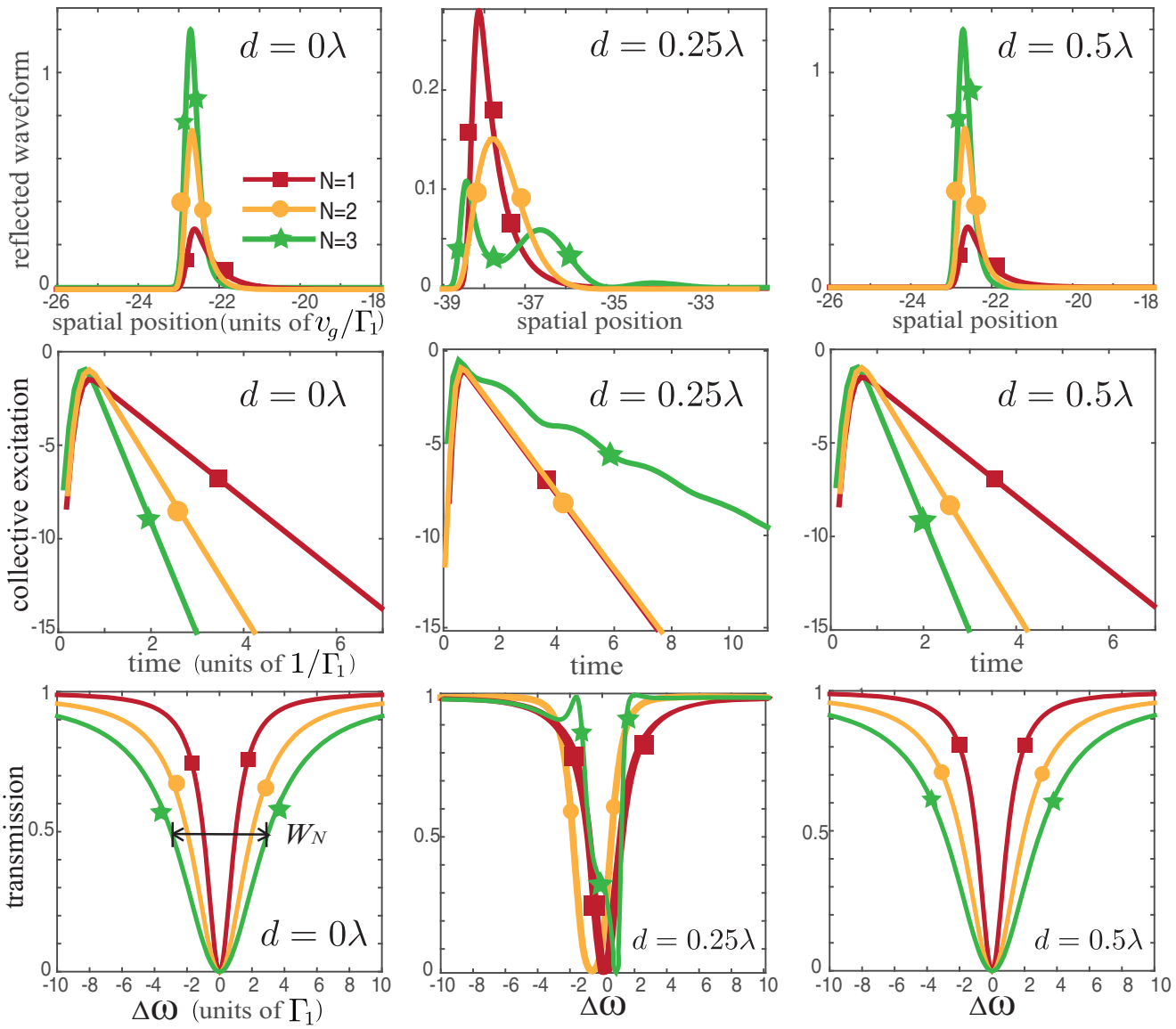

FIG. 2. Responses of an N-atom ensemble interacting with a single photon pulse: $N=1$ (red, square symbol), 2 (orange, round symbol), and 3 (green, star symbol). Left column ($d=0\lambda$): (upper panel) reflected wave form, origin at x_1; (center panel) collective excitation $\sum_{n=1}^{N}|e_{na}(t)|^2$ (in $\log_e$ scale); and (lower panel) transmission spectrum. Center column: $d=0.25\lambda$. Right column: $d=0.5\lambda$. $\Delta\omega$ is the detune from the transition frequency.

of x_0 is irrelevant). $k_0 = \Omega_1/v_g$ is the center frequency of the photon, which is on resonance with the atoms. When the photon is incident upon the atomic cloud in its ground state, the numerical results are presented in Figs. 2 and 3. In Fig. 2, we vary the number of atoms N and the distance d ($d = M\lambda/2$) between them. In the left column of Fig. 2 ($d = 0\lambda$ and $M = 0$), the reflected single-photon wave peaks increasingly sharper when N increases, indicating the emergence of single-photon superradiance (upper panel). The collective excitation (center panel) $\sum_{n=1}^{N} |e_{na}(t)|^2$ undergoes an exponential decay with a collective emission rate $\Gamma_N = N\Gamma_1$ numerically, and the state of atoms is a symmetric state, $\bar{e}(t)\sum_{n=1}^{N} a_{ne}^{\dagger} a_{ng}|0,-\rangle/\sqrt{N}$, in agreement with theoretical predictions. The transmission spectra (lower panel) all have a Lorentzian shape with a FWHM $W_N = NW_1$ numerically. Thus we have numerically demonstrated the single-photon superradiance. In the center column of Fig. 2 ($d = 0.25\lambda$ and $M = 0.5$, not an integer), the amplitude of the reflected single-photon wave now decreases and distorts when the number of atoms increases. The burst emission is absent in this case. The long-time decay rates of collective excitations for $N = 1$ and $N = 2$ are the same. The collective excitation for the $N = 3$ case wiggles and slows down, indicating the photonic interference due to the finite distance between the atoms. The transmission spectra for $N = 2$ and $N = 3$ are non-Lorentzian. In the right column of Fig. 2 ($d = 0.5\lambda$ and $M = 1$), all quantities in Fig. 2 are identical to those of the $d = 0\lambda$ case, but the atomic state is different and becomes a staggered state, $\bar{e}(t)\sum_{n=1}^{N}(-1)^{n-1} a_{ne}^{\dagger} a_{ng}|0,-\rangle/\sqrt{N}$. The numerical results are in agreement with the aforementioned theoretical discussions.

The cooperative emission of a group of quantum emitters applies equally to both atoms and artificial atoms [25,26]. In recent years, significant effort has been devoted to generating quantum optical phenomena in solid state platforms. Multiphoton superradiance from artificial atoms has been experimentally demonstrated [27–29]. Theoretical aspects of superradiance from two artificial atoms have been considered using input-output formalism [30]. Here we use a Hamiltonian-based approach to numerically investigate the more general scenarios that are directly relevant to current single-photon superradiance experiments using artificial atoms.

Figure 3(a) presents the numerical investigations for the single-photon superradiance when deviations in transition frequencies (upper row) and in decay rates (lower row) are present in the artificial atoms. In the upper row of Fig. 3, we investigate three collocated artificial atoms. In practice, the deviations in transition frequencies approximately follow a Gaussian distribution. Three cases with different standard deviation σ are studied. To mimic the worst scenario, the spectral distances between transition frequencies of artificial atoms are chosen to be on the order of the standard deviation. The incident photon is tuned to be on resonance with the first artificial atom. Also, the bandwidth of the photon is taken to be ten times the single atom decay rate Γ_1. In case I, the deviation is 3% of the center frequency ($\sim 10^6\Gamma_1$), which is far larger than the bandwidth of the photon [see Fig. 3(b), configuration I, for the placement of all bandwidths]. In this case, the two far-detuned artificial atoms outside of the photon bandwidth do not interact with the photon and appear to be transparent to the photon. Thus the responses of the three-artificial atom cloud [red curves with square symbols in the upper row of Fig. 3(a)] are the same as those of the one-atom case in Fig. 2. In case II, the deviation is reduced to be smaller than the bandwidth of the photon [$\sigma = 3\Gamma_1$, see Fig. 3(b), configuration II, for bandwidth placement]. Now

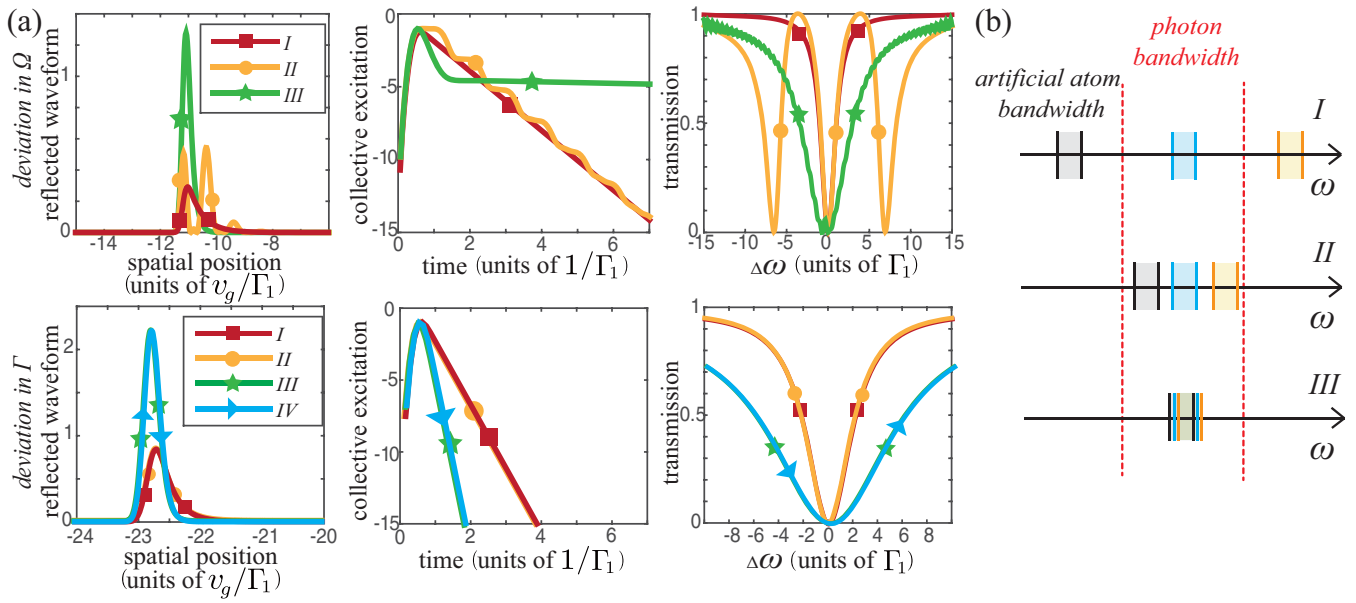

FIG. 3. (a) Responses of an ensemble of artificial atoms, including the reflected wave form, the collective excitation (in $\log_e$ scale), and the transmission spectrum. Upper row: Deviations in transition frequency. Case I: $\sigma = 3\%$ of the center frequency; case II: $\sigma = 3\Gamma_1$; case III: $\sigma = 0.5\Gamma_1$. Lower row: Deviations in decay rates. Case I: $\Gamma^{(1)} = 0.8\Gamma_1$ and $\Gamma^{(2)} = 1.4\Gamma_1$; case II: $\Gamma^{(1)} = \Gamma_1$ and $\Gamma^{(2)} = 1.2\Gamma_1$; case III: $\Gamma^{(1)} = \Gamma_1$ and $\Gamma^{(2)} = 5\Gamma_1$; case IV: $\Gamma^{(1)} = \Gamma_1$, $\Gamma^{(2)} = 2\Gamma_1$, and $\Gamma^{(3)} = 3\Gamma_1$ (three artificial atoms). (b) Placement of the photon's and the artificial atoms' bandwidths for the first row in panel (a) (not to scale).

the three artificial atoms interact with different frequency components of the photon. So that the reflected photon wave form (orange curve with round symbols) exhibits several peaks. Such a beating phenomenon is a direct consequence of the interference between those frequency components, and it is also visible in the collective excitation. The transmission spectrum has three dips, corresponding to the three atomic transition frequencies. These results also confirm that the effective mapping does not hold for this case. In case III, the deviation is further decreased to be $0.5\Gamma_1$. The artificial atoms now interact with essentially the same frequency component in the photon bandwidth [see Fig. 3(b), configuration III]. Now the reflected photon wave (green curve with star symbols) exhibits superradiance. The collective excitation exhibits a speed-up decay in the short-time limit, indicating the single-photon superradiance, and becomes flat in the long-time limit (albeit small), as a tiny portion of the photonic wave is trapped between atoms. As the detuning is small, the effective mapping is approximately valid; so the single-photon superradiance is present in this case. In real experiments, the decay rate usually has a value of 0.1–100 MHz. For the artificial atoms operating at an optical frequency of 200–1000 THz, to fulfill the relation shown in Fig. 3(b), configuration III, the deviation of transition frequencies must be controlled within 0.0001% to observe single-photon superradiance. For a microwave frequency of 5–10 GHz, the required deviation is not hard to achieve, which is about 1%.

Next, for cases of varying decay rates, when the distance between atoms is $M\lambda/2$ (M is an integer), by a direct generalizing of the previous effective mapping procedure, we could prove that an effective mapping still holds and the superradiant emission rate scaling $\Gamma_N = \overline{\Gamma} = \sum_{n=1}^{N} \Gamma^{(n)}$ ($\Gamma^{(n)}$ denotes the decay rate of the nth atom), regardless of the individual decay rate and the total atom number N. We numerically demonstrate this relation by simulating four cases. In cases I and II, we keep the atom number ($N = 2$) and the total decay rate fixed, but the individual decay rate can be different otherwise. In cases III and IV, the atom number is different, but the total decay rate is still kept same. The numerical results are in agreement with those from an effective two-level system.

In this article, we present a quantitative investigation for single-photon superradiance, in both the time and the frequency domain. One of our results provides a recipe for enhancing the decay rate of an atomic cloud. In any quantum optical device, the rate for processing photons is fundamentally limited by the decay rate of qubits. The processing rate is around 1 GHz for qubits with $\Gamma_1 = 10^8$–10^9 Hz. Our work could facilitate the design of ultrafast quantum optical devices for ultrahigh bit rate operations for quantum information science.

This work was supported in part by NSF ECCS Grant No. 1608049.

[1] M. Gross and S. Haroche, Phys. Rep. **93**, 301 (1982).
[2] R. H. Dicke, Phys. Rev. **93**, 99 (1954).
[3] A. A. Svidzinsky, F. Li, H. Li, X. Zhang, C. H. R. Ooi, and M. O. Scully, Phys. Rev. A **93**, 043830 (2016).
[4] A. T. Black, J. K. Thompson, and V. Vuletić, Phys. Rev. Lett. **95**, 133601 (2005).
[5] R. Röhlsberger, K. Schlage, B. Sahoo, S. Couet, and R. Rüffer, Science **328**, 1248 (2010).
[6] E. M. Kessler, S. Yelin, M. D. Lukin, J. I. Cirac, and G. Giedke, Phys. Rev. Lett. **104**, 143601 (2010).
[7] R. A. de Oliveira, M. S. Mendes, W. S. Martins, P. L. Saldanha, J. W. R. Tabosa, and D. Felinto, Phys. Rev. A **90**, 023848 (2014).
[8] S. Ritter, C. Nolleke, C. Hahn, A. Reiserer, A. Neuzner, M. Uphoff, M. Mucke, E. Figueroa, J. Bochmann, and G. Rempe, Nature (London) **484**, 195 (2012).
[9] X. Li, Y. Wu, D. Steel, D. Gammon, T. H. Stievater, D. S. Katzer, D. Park, C. Piermarocchi, and L. J. Sham, Science **301**, 809 (2003).
[10] J. R. Petta, A. C. Johnson, J. M. Taylor, E. A. Laird, A. Yacoby, M. D. Lukin, C. M. Marcus, M. P. Hanson, and A. C. Gossard, Science **309**, 2180 (2005).
[11] M. O. Scully and A. A. Svidzinsky, Science **325**, 1510 (2009).
[12] U. van Bürck, D. P. Siddons, J. B. Hastings, U. Bergmann, and R. Hollatz, Phys. Rev. B **46**, 6207 (1992).
[13] L.-M. Duan, M. D. Lukin, J. I. Cirac, and P. Zoller, Nature (London) **414**, 413 (2001).
[14] N. Skribanowitz, I. P. Herman, J. C. MacGillivray, and M. S. Feld, Phys. Rev. Lett. **30**, 309 (1973).
[15] M. Gross, C. Fabre, P. Pillet, and S. Haroche, Phys. Rev. Lett. **36**, 1035 (1976).
[16] A. Goban, C.-L. Hung, S.-P. Yu, J. D. Hood, J. A. Muniz, J. H. Lee, M. J. Martin, A. C. McClung, K. S. Choi, D. E. Chang, O. Painter, and H. J. Kimble, Nat. Commun. **5**, 3808 (2014).
[17] A. Goban, C.-L. Hung, J. D. Hood, S.-P. Yu, J. A. Muniz, O. Painter, and H. J. Kimble, Phys. Rev. Lett. **115**, 063601 (2015).
[18] J. T. Shen and S. Fan, Opt. Lett. **30**, 2001 (2005).
[19] Z. Chen, Y. Zhou, and J.-T. Shen, Opt. Lett. **42**, 887 (2017).
[20] J.-T. Shen and S. Fan, Phys. Rev. A **79**, 023837 (2009).
[21] Y. Zhou, Z. Chen, and J. T. Shen (unpublished).
[22] J.-T. Shen and S. Fan, Phys. Rev. Lett. **95**, 213001 (2005).
[23] D. E. Chang, L. Jiang, A. V. Gorshkov, and H. J. Kimble, New J. Phys. **14**, 063003 (2012).
[24] S. Das, G. S. Agarwal, and M. O. Scully, Phys. Rev. Lett. **101**, 153601 (2008).
[25] P. Tighineanu, R. S. Daveau, T. B. Lehmann, H. E. Beere, D. A. Ritchie, P. Lodahl, and S. Stobbe, Phys. Rev. Lett. **116**, 163604 (2016).
[26] A. González-Tudela and D. Porras, Phys. Rev. Lett. **110**, 080502 (2013).
[27] J. A. Mlynek, A. A. Abdumalikov, C. Eichler, and A. Wallraff, Nat. Commun. **5**, 5186 (2014).
[28] V. V. Temnov and U. Woggon, Phys. Rev. Lett. **95**, 243602 (2005).
[29] M. Scheibner, T. Schmidt, L. Worschech, A. Forchel, G. Bacher, T. Passow, and D. Hommel, Nat. Phys. **3**, 106 (2007).
[30] K. Lalumière, B. C. Sanders, A. F. van Loo, A. Fedorov, A. Wallraff, and A. Blais, Phys. Rev. A **88**, 043806 (2013).